Journal of Alloys and Compounds 506 (2010) 734–738

Contents lists available at ScienceDirect

Journal of Alloys and Compounds

journal homepage: www.elsevier.com/locate/jallcom

Synthesis and mechanical properties of nano-layered composite

Guobing Ying[a], Xiaodong He[a,*], Mingwei Li[b], Yibin Li[a], Shanyi Du[a]

[a] Center for Composite Materials and Structures, Harbin Institute of Technology, Harbin 150080, China
[b] National Key Lab for Precision Hot Processing of Metal, Harbin Institute of Technology, Harbin 150001, China

ARTICLE INFO

Article history:
Received 19 May 2010
Received in revised form 4 July 2010
Accepted 7 July 2010
Available online 15 July 2010

Keywords:
Ti_3AlC_2
Cr_2AlC
$M_{n+1}AX_n$
SHS/PHIP
Mechanical properties

ABSTRACT

In this paper, the bulk nano-layered composite, which contains Ti_3AlC_2, Cr_2AlC and TiC, has been synthesized by self-propagating high-temperature synthesis with the pseudo-hot isostatic pressing process (SHS/PHIP). The density, hardness, flexural strength and fracture toughness of the fully dense composite are $4.55 \pm 0.02\ g/cm^3$, 10.53 ± 0.48 GPa, 592 ± 25 MPa and $6.23 \pm 0.35\ MPa\ m^{1/2}$, respectively. The nano-layered composite exhibits a high hardness, flexural strength, and fracture toughness due to the toughening of the overlap joint lamellas of the Ti_3AlC_2–Cr_2AlC phases and the strengthening of the homogeneously dispersed fine TiC particles.

1. Introduction

As the member of the layered ternary $M_{n+1}AX_n$ phases (where $n = 1, 2, 3$, M is an early transition metal, A is a IIIA or IVA element and X is C or N), Ti_3AlC_2 and Cr_2AlC possess a unique combination of the properties of both ceramics and metals: readily machinable, thermal and electrical conductive, thermal shock and high-temperature oxidation resistant, damage tolerant, lightweight, and elastically stiff [1–5].

However, the weaknesses such as low hardness and unsatisfied strength limit their widespread applications. Considerable efforts to strengthening of MAX phases, second phase formed from quaternary system needs to be incorporated for forming a composite. Li et al. [6] synthesized the Ti_3AlC_2/TiB_2 composite using Ti, Al, graphite and B_4C powders as raw materials, and it exhibits higher mechanical properties when compared with the Ti_3AlC_2 ceramic. Also Ti_2AlC–Ti_3AlC_2–Ti_3SiC_2 composite, Ti_3SiC_2–TiC composite and $Ti_3Si(Al)C_2/SiC$ composite successfully formed from Ti–Si–Al–C system are reported by Hong et al. [7], Zhang et al. [8] and Wan et al. [9], respectively. The most possible MAX phases in Ti–Al–C system are Ti_3AlC_2 and Ti_2AlC [10]. Cr_2AlC has been identified to be the only MAX phase in the Cr–Al–C system [5,11]. Thus, the coexistence of these phases and other binary carbides (such as TiC) in a Ti–Cr–Al–C system composite is possible. And a composite formed from this system would improve the mechanical properties compared with the monolithic MAX phase ceramic. It is reported that the 1.5Ti–0.5Cr–Al–C system presents the possible composite and the coexistence of the TiC and MAX phases [12]. However, the resultant 1.5Ti–0.5Cr–Al–C product by SHS method still needs to be investigated: bulk densification, phase composition and properties.

In this paper, bulk (Ti_3AlC_2–Cr_2AlC)/TiC nano-layered composite was attempted to synthesize by SHS/PHIP, using Ti, Cr, Al, and carbon black powders as raw materials. The phase composition and microstructure of the composite were investigated. The density and room-temperature mechanical properties such as Vickers hardness, flexural strength, and fracture toughness of the composite were determined through various techniques.

2. Experimental procedure

Titanium (<45 μmØ, 99.4% purity), chromium (<45 μmØ, 99.0% purity), aluminium (<29 μmØ, 99.7% purity) and carbon black (≈7 μmØ, 99.0% purity) powders were used as the raw materials. The powders with the stoichiometric ratios of Ti:Cr:Al:C 1.5:0.5:1:1 were mixed by planetary mill in absolute alcohol for 12 h. The ZrO_2 ball was used as milling media. The mixed powders were dried by the rotary vacuum evaporator after being sieved. Then the powder mixtures were compacted uniaxially in a die. The powder mixtures were hold at a pressure of 20 MPa for 30 s, using the mold with a 55 mm in diameter and 200 mm in height. Then the pre-compacted block was put in an 75 μmØ mold. Resistance wire filled with amorce was used as the portfire and was put under the pre-compacted block. Sand was used as the medium of the pseudo-hot isostatic pressing process. The W–Re5/26 thermocouple was embedded into the sample. A temperature recorder with a 0.2 s picking cycle was used to collect the temperature data. The SHS reaction generated after ignition. Then the SHS sample was obtained by the reaction of the pre-compacted block. After the system arrived at the point of adiabatic combustion temperature $T_{ad,}$ it was kept upon 1600 K for 25 s. A 225 MPa PHIP pressure was forced on the pressure head, in which the dwell time was set as 25 s. The SHS/PHIP process details could be found elsewhere [13].

* Corresponding author. Tel.: +86 451 86412513; fax: +86 451 86402333.
E-mail address: hexd@hit.edu.cn (X. He).

0925-8388/$ – see front matter © 2010 Elsevier B.V. All rights reserved.
doi:10.1016/j.jallcom.2010.07.057

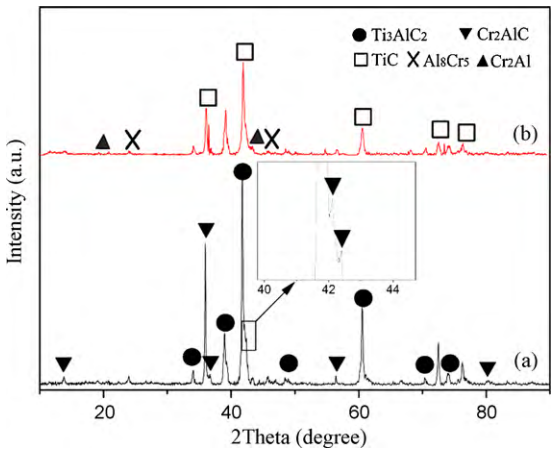

Fig. 1. X-ray diffraction patterns of the samples prepared by (a) SHS and (b) SHS/PHIP.

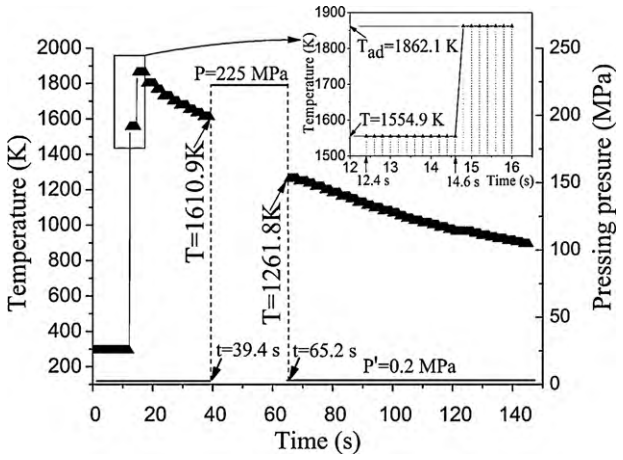

Fig. 2. The temperature and pressing pressure variation in the SHS/PHIP process.

Powders porphyrized from the products were used for the XRD analysis. In the Rietveld method, the XRD pattern was determined by XRD (RINT2000 vertical goniometer, Japan) with Cu Kα radiation at 40 kV and 30 mA at a scanning speed of 0.02°/s. SEM (HITACHI S-4700, Japan) was used to observe the microstructure of the samples. A 2% HNO_3–HF solution was used as the corrosion medium of he polished surface of the samples. The elements of the phases were evaluated by the energy dispersive spectrometer, EDS, (EDAX, AMETEK). The density of the synthesized sample was measured by the Archimedes principle. Vickers hardness data were determined by Micro-586 equipment using the loads of 1 N, 2 N, 5 N and 10 N, respectively. Flexural strength at room-temperature was measured in three-point bending at a cross head speed of 0.5 mm/min, using parallelepipeds with dimensions of 4 × 3 × 36 mm. Fracture toughness was measured using the method of single edge notched beam (SENB), and 2 × 4 × 22 mm parallelepipeds with 2 mm notch were measured using a speed of 0.05 mm/min.

3. Results and discussion

3.1. Phases composition

The XRD patterns of the samples prepared by SHS and SHS/PHIP is shown in Fig. 1. It is detected that Ti_3AlC_2 (JCPDS 52-0875), Cr_2AlC (JCPDS 29-0017) and TiC (JCPDS 32-1383) phases with unwanted Cr_2Al and Al_8Cr_5 compounds are identified in the XRD patterns. Reports show there have $Ti_3Al_{1-x}Si_xC_2$ [14], $Ti_3Si_{0.5}Al_{0.5}C_2$ [15], $Ti_3Si_{0.9}Al_{0.1}C_2$ [16], $Ti_2Al(C_{0.5},N_{0.5})$ [17], $Ti_3Al(C_{0.5},N_{0.5})$ [17], and the M-site solid solutions such as $(V,Cr)_3AlC_2$ [18] and $(V,Cr)_2AlC$ [18,19]. And the solid solutions could solution strength the composite [14–19], but there's no M-site solid solutions is detected in the samples. It is explained by the larger atomic size and valence electrons differences between Cr and Ti, which leads to less phase stability of M-site solid solutions [4,20]. It is reported that the unwanted Cr_2Al and Al_8Cr_5 are also found in Cr_2AlC synthesized by hot pressing [4,5,21]. But there's no Cr_2Al is detected in the SHS/PHIP sample. Crystal structure and peak profile parameters are refined by using a DBWS code in Cerius computational program for materials research [6]. Based upon the Chung F.H. method [22], the contents of Ti_3AlC_2, Cr_2AlC, TiC and Al_8Cr_5 formed in the bulk composite are estimated from the refined XRD peak intensities according to the following formula:

$$W_{Ti_3AlC_2} = \frac{I^{Ti_3AlC_2}_{(104)}}{I^{Ti_3AlC_2}_{(104)} + 0.868I^{Cr_2AlC}_{(103)} + 1.351I^{TiC}_{(200)} + 1.095I^{Al_8Cr_5}_{(303)}} \quad (1)$$

$$W_{Cr_2AlC} = \frac{I^{Cr_2AlC}_{(103)}}{I^{Cr_2AlC}_{(103)} + 1.152I^{Ti_3AlC_2}_{(104)} + 1.597I^{TiC}_{(200)} + 1.261I^{Al_8Cr_5}_{(303)}} \quad (2)$$

$$W_{TiC} = \frac{I^{TiC}_{(200)}}{I^{TiC}_{(200)} + 0.74I^{Ti_3AlC_2}_{(104)} + 0.643I^{Cr_2AlC}_{(103)} + 0.811I^{Al_8Cr_5}_{(303)}} \quad (3)$$

$$W_{Al_8Cr_5} = \frac{I^{Al_8Cr_5}_{(303)}}{I^{Al_8Cr_5}_{(303)} + 0.913I^{Ti_3AlC_2}_{(104)} + 0.793I^{Cr_2AlC}_{(103)} + 1.234I^{TiC}_{(200)}} \quad (4)$$

where $W_{Ti_3AlC_2}$, W_{Cr_2AlC}, W_{TiC} and $W_{Al_8Cr_5}$ are the mass fractions of Ti_3AlC_2, Cr_2AlC, TiC and Al_8Cr_5, respectively. $I^{Ti_3AlC_2}_{(104)}$, $I^{Cr_2AlC}_{(103)}$, $I^{TiC}_{(200)}$, and $I^{Al_8Cr_5}_{(303)}$ are the integrated diffraction intensities of the Ti_3AlC_2(1 0 4), Cr_2AlC(1 0 3), TiC(2 0 0) and Al_8Cr_5(3 0 3) peaks, respectively. The results of the XRD phase analysis of synthetic (Ti_3AlC_2–Cr_2AlC)/TiC composite are listed in Table 1. According to the result of XRD analysis, the density of the composite is calculated as 4.6743 g/cm^3.

The measured temperature and pressing pressure variation in the SHS/PHIP process is given in Fig. 2. The adiabatic combustion temperature T_{ad} is measured as 1862.1 K (t = 14.8 s). The T_{ad} is higher than the decomposed temperature of Ti_3AlC_2 (1723 K [10]) and Cr_2AlC (1773 K [23]). So, Ti_3AlC_2 and Cr_2AlC were synthesized while the system is cooling. The 225 MPa pressure of the PHIP process is measured to start when it reached 1610.9 K, and kept on for 25.8 s. This point is slightly lower than the 1673 K for Ti_3AlC_2 [24] and the 1673 K for Cr_2AlC [5,11,25] prepared by hot pressing. It is reported that Ti–Al melt and TiC crystallites are firstly formed during the combustion of Ti_3AlC_2 in Ti–Al–C system, and TiC would dissolve into the Ti–Al melt and then grow into layered Ti_3AlC_2 [10]. Ti–Al intermetallic compounds are frequently found in the Ti–Al–C system. However, there's no Ti–Al intermetallic compound in this Ti–Cr–Al–C system. The Cr–Al intermetallic compound other than Ti–Al intermetallic compound in the sample reflects the two facts.

Table 1
Summary of the X-ray phase analysis of synthetic (Ti_3AlC_2–Cr_2AlC)/TiC composite.

Phase composition	Crystal structure	Lattice constants (Å)	Theoretic density (g/cm^3)	Content (wt.%)	Content (vol.%)
Ti_3AlC_2	$P6_3/mmc$ Hexagonal	a = 3.07(14), c = 18.53(61)	4.27(01)	39.5	43.24
Cr_2AlC	$P6_3/mmc$ Hexagonal	a = 2.85(62), c = 12.85(79)	5.22(71)	25.7	22.98
TiC	Fm–3m (2 2 5) Cubic	a = 4.31(92)	4.93(86)	29.5	27.92
Al_8Cr_5	$R3m$ (1 6 0) Hexagonal	a = 12.75(05), c = 7.96(23)	4.22(88)	5.3	5.86

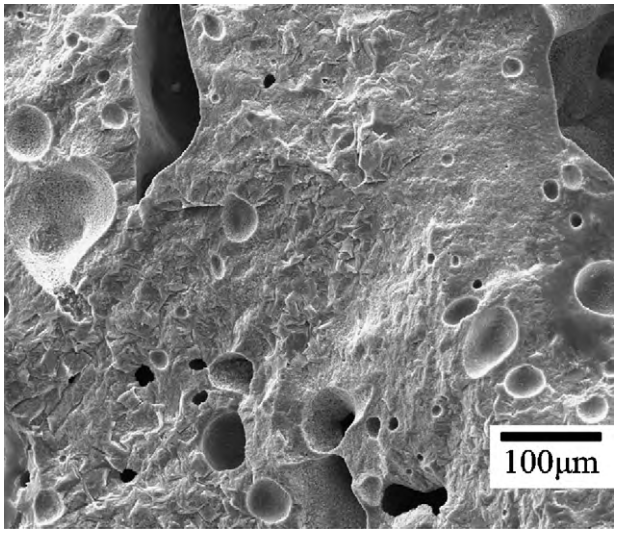

Fig. 3. SEM photograph of the fracture surface of the porous SHS sample.

First, if Cr–Al melt and Ti–Al melt were formed before the formation of MAX phases, the Gibbs energy of the Cr–Al intermetallic compound (as the Al_8Cr_5 [26], at the high-temperature) is lower than the Ti–Al intermetallic compound of Ti_3Al [10]. And it is inclined to form Cr–Al intermetallic compound. Second is the firstly formed TiC adequately consumed and reacted with the Ti–Al melt.

3.2. Microstructure observation

A typical SEM micrograph of the fracture surface of the SHS sample is shown in Fig. 3, which reveals many holes in the sample. A possibility of this SHS sintering phenomenon may due to the C reducing atmosphere. Another possibility is caused by the high vapor pressure of Al. The typical SEM micrograph of the fracture surface of the SHS/PHIP sample is shown in Fig. 4(a). The density of bulk SHS/PHIP sample is $4.55 \pm 0.02\,g/cm^3$ (97.34% of the $4.6743\,g/cm^3$ calculated by XRD analysis), which is 115% larger than that of the porous SHS sample ($2.11\,g/cm^3$). The high dense of the composite may be due to the Al-melt during the synthesis process. Cleavage planes could be observed in the bulk SHS/PHIP sample. The cleavage planes are alternately tore into about 50 nm layer, which confirms the nano-layered of MAX phases, as shown in Fig. 4(b).

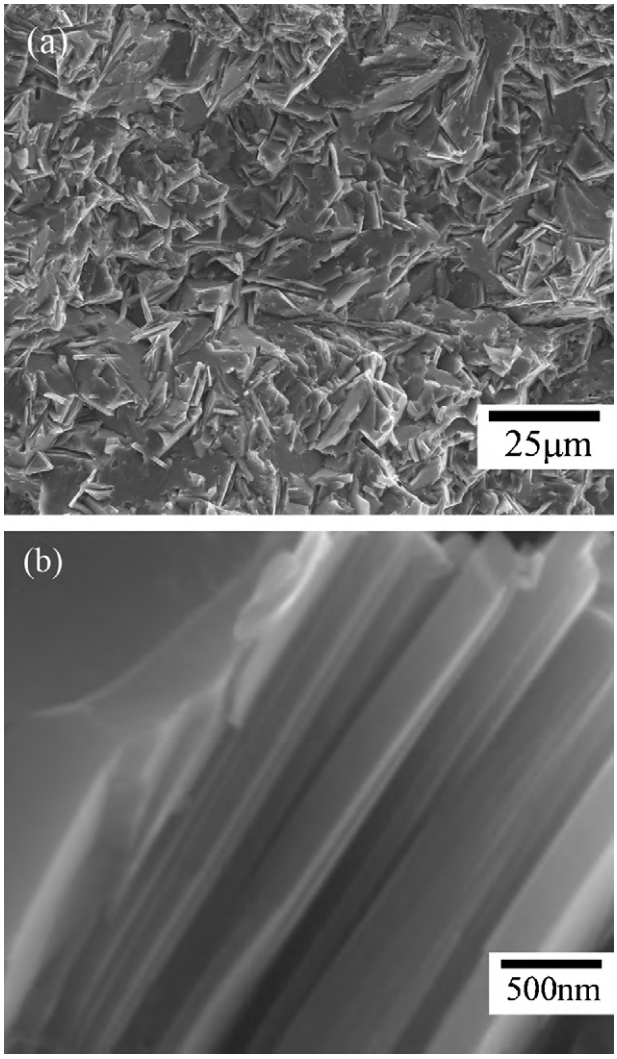

Fig. 4. (a) The SEM photograph of the fracture surface and (b) the typical nano-layered structure in the SHS/PHIP sample.

The Ti_3AlC_2–Cr_2AlC phases uniformly distribute in the sample, in which the interface are dispersed with TiC particles, as given in Fig. 5(a)–(c). The diameter of the TiC particles is about 1 μm. There have disaccord Ti_3AlC_2–Cr_2AlC phases are Ti–Al–C rich phases with

Table 2
Comparison of fabrication details and mechanical properties.

Comparison items	$Ti_3Al_{1.1}C_{1.8}$ [24] Ti_3AlC_2 [27]	Cr_2AlC	Ti_3AlC_2/TiC –Al_2O_3 composite	This work
Fabrication methods	HIP [24], HP [27]	HP [4,5,11,21,25,28]	CS + HP [30]	SHS/PHIP
Raw materials	Ti, graphite, Al_4C_3 [24]; Ti, Al, graphite [27]	Cr, Al, Cr_7C_3, Cr_3C_2 [25]; Cr, Al, graphite [4,5,11,21,28]	TiO_2, Al, graphite [30]	Ti, Cr, Al, carbon black
Synthesis temperature (°C)	1600 [24], 1500 [27]	1400 [4,5,11,25,28], 1330 [21]	1500 [30]	–
Holding time	16 h [24] 5 min [27]	1 h [4,11,21,25,28], 30 min [5]	30 min [30]	25 s
Applied pressure (MPa)	70 [24], 25 [27]	20 [25], 30 [4,5,11,28]	10 [30]	225
Impurity phase	Al_2O_3 [24], none [27]	Cr_7C_3 [11,21,25,28], Cr_2Al [21], Al_8Cr_5 [21]	Al_3Ti [30]	Cr_2Al, Al_8Cr_5
Procedure	Complicated [24], simple [27]	Simple [4,11,21,25,28]	Simple [30]	Very simple
Cost	High [24], low [27]	Low [4,11,21,25,28]	Low [30]	Very low
Density (g/cm^3)	4.2 [24]	5.1 [11], 5.2 [25], 5.21 [28]	–[a]	4.55 ± 0.02
Vichers hardness (GPa)	3.5 [24] 2.5–4.7 [27]	5.2 [11], 5.5 [5], 3.3–5.5 [4], 3.5 [28]	13.3 ± 1.1 [30]	10.53 ± 0.48
Flexural strength (MPa)	375 ± 15 [24], 340 [27]	494 ± 22 [25], 483 ± 29 [11], 378 [28]	466 ± 39 [30]	592 ± 25
Fracture toughness ($MPa \cdot m^{1/2}$)	7.2 [27]	5.8 [4]	5.8 ± 0.3 [30]	6.23 ± 0.35

[a] Not reported.

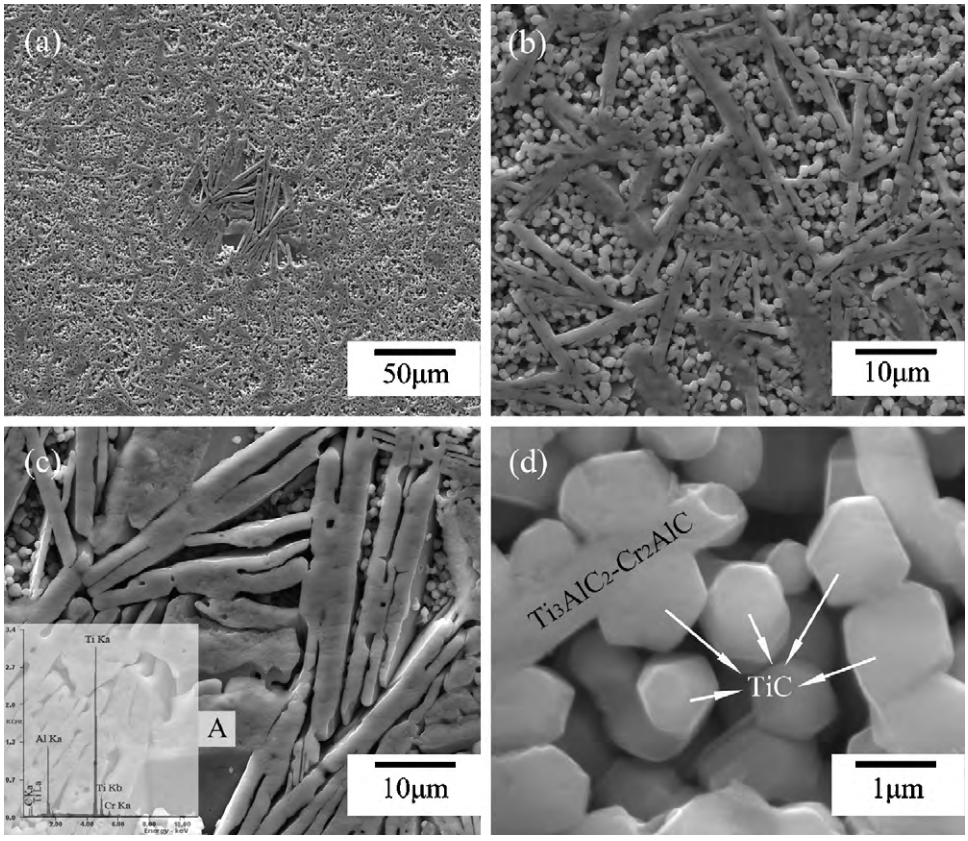

Fig. 5. (a) SEM photograph of the corrosion polished surface of the SHS/PHIP sample and (b) uniform distributed Ti_3AlC_2–Cr_2AlC and TiC phases. (c) The disaccord Ti_3AlC_2–Cr_2AlC phase in the samples (inset is the EDS of zone A) and (d) single-size TiC with about 1 μm diameter.

little Cr, as shown in the inset EDS of zone A in Fig. 5(c). It is clear that there's more Ti_3AlC_2 other than Cr_2AlC in this place. Because the SHS/PHIP process last no more than 60 s and the phase formed after the reaction, the diffusion time is inadequate. The disaccord start composition in located place would result in a phases uniformly distribute in the sample. It is indicated that the firstly formed phases are in situ synthesized. It is interesting to find that there have special 'Y' and 'H' shaped overlap joint lamellas, as shown in Fig. 5(b) and (c). And the most important reveal of the special 'Y' and 'H' is that the composite is composed of uniform distributed overlap joint lamellas, and each lamella is composed of nano-layered Ti_3AlC_2–Cr_2AlC phases.

3.3. Mechanical properties

The comparison of fabrication details and mechanical properties between the reported materials and the present composite are listed in Table 2. The Vickers hardness values of the nano-layered composite are given in Fig. 6. It is reported that the elastic recovery produced a smaller indent after indentation result in a high Vickers hardness at low indentation loads [5]. The measured Vickers hardness of the composite at the load of 10 N is 10.53 ± 0.46 GPa, which is significantly higher than the high purity single phase Ti_3AlC_2 (3.5 GPa [24], 2.5–4.7 GPa [27]) and Cr_2AlC (5.2 GPa [11], 5.5 GPa [5], 3.3–5.5 GPa [4] and 3.5 GPa [28]) compound. It is reported that the Vickers hardness of TiC is about 28.5–33.5 GPa [29], which is much larger than that of Ti_3AlC_2 or Cr_2AlC. It indicates that the fine particle TiC has an intensively strengthening effect on the composite. The flexural strength at room-temperature is 592 ± 25 MPa, which is higher than that of Ti_3AlC_2 (375 ± 15 MPa [24], 340 MPa [27]) and Cr_2AlC (494 ± 22 MPa [25], 483 ± 29 MPa [11] and 378 MPa [28]). However, the fracture toughness is 6.23 ± 0.35 MPa $m^{1/2}$, which is lower than that of Ti_3AlC_2 (7.2 MPa $m^{1/2}$ [27]), but still slight higher than Cr_2AlC (5.8 MPa $m^{1/2}$ [4]). For the Ti_3AlC_2/TiC–Al_2O_3 composite reported by Chen et al. [30], the hardness, flexural strength and toughness are, respectively, 10.53 ± 0.48 MPa [30], 466 ± 39 MPa [30] and 5.8 ± 0.3 MPa $m^{1/2}$ [30]. Compared with the Ti_3AlC_2/TiC–Al_2O_3 composite, the difference between the Ti_3AlC_2/TiC–Al_2O_3 and (Ti_3AlC_2–Cr_2AlC)/TiC is the incorporating of the Cr_2AlC (replaced Al_2O_3) into the Ti_3AlC_2–TiC. And a remarkable flexural strength and a higher toughness indicate that the Cr_2AlC exhibits toughening and strengthening effect. The improvement in the mechanical properties can be mainly ascribed to the contribution of homogeneously dispersed fine TiC particles and overlap joint lamellas of the Ti_3AlC_2–Cr_2AlC phases.

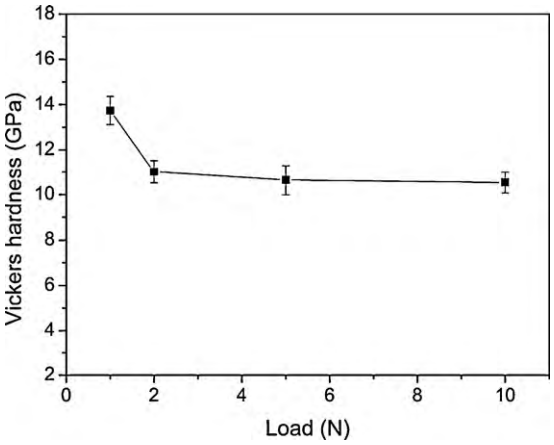

Fig. 6. Effect of indentation loads on the Vickers hardness.

4. Conclusions

The bulk nano-layered composite has been successfully synthesized by SHS/PHIP. The phase composition of SHS sample and SHS/PHIP sample was investigated. The composite is composed of uniform distributed overlap joint lamellas and fine particle TiC (about 1 μm), and each lamella is composed of nano-layered (with the thickness of 50 nm) Ti_3AlC_2–Cr_2AlC phases. The formation of the MAX phases is detected as in situ synthesis while the system is cooling. The density of compacted SHS/PHIP is $4.55 \pm 0.02\ g/cm^3$, which is 115% larger than that of the $2.11\ g/cm^3$ of the SHS porous sample. The hardness, flexural strength, and fracture toughness of the SHS/PHIP compacted sample are 10.53 ± 0.48 GPa, 592 ± 25 MPa, $6.23 \pm 0.35\ MPa\ m^{1/2}$, respectively. Due to the toughening of the overlap joint lamellas of the Ti_3AlC_2–Cr_2AlC phases and the strengthening of the homogeneously dispersed fine TiC particles, the nano-layered composite exhibits a high hardness, flexural strength, and fracture toughness.

Acknowledgement

Discussion on refine the language with Ph.D. Zhang Binbin (HEU, China) is gratefully acknowledged. This article was supported by the Major Research Plan of the National Natural Science Foundation of China (Grant No. 90816005).

References

[1] W.B. Tian, P.L. Wang, Y.M. Kan, G.J. Zhang, J. Alloy Compd. 461 (2008) L5–L10.
[2] Y. Zou, Z.M. Sun, H. Hashimoto, S. Tada, J. Alloy Compd. 456 (2008) 456–460.
[3] M.W. Barsoum, T. Zhen, S.R. Kalidindi, M. Radovic, A. Murugaiah, Nat. Mater. 2 (2003) 107–111.
[4] Z.J. Lin, Y.C. Zhou, M.S. Li, J. Mater. Sci. Technol. 23 (2007) 721–746.
[5] Z.J. Lin, Y.C. Zhou, M.S. Li, J.Y. Wang, Z. Metallkd. 96 (2005) 291–296.
[6] C. Li, M. Li, Y. Zhou, J. Zhang, L. He, J. Am. Ceram. Soc. 90 (2007) 3615–3620.
[7] X.L. Hong, B.C. Mei, J.Q. Zhu, W.B. Zhou, J. Mater. Sci. 40 (2005) 2749–2750.
[8] J.F. Zhang, L.J. Wang, W. Jiang, L.D. Chen, Mater. Sci. Eng. A 487 (2008) 137–143.
[9] D.T. Wan, Y.C. Zhou, Y.W. Bao, C.K. Yan, Ceram. Int. 32 (2006) 883–890.
[10] Z.B. Ge, K.X. Chen, J.M. Guo, H.P. Zhou, J.M.F. Ferreira, J. Eur. Ceram. Soc. 23 (2003) 567–574.
[11] W.B. Tian, P.L. Wang, G.J. Zhang, Y.M. Kan, Y.X. Li, J. Am. Ceram. Soc. 90 (2007) 1663–1666.
[12] E.A. Levashov, Y.S. Pogozhev, D.V. Shtansky, M.I. Petrzhik, Russ. J. Non-Ferr. Met. 50 (2009) 151–159.
[13] Y.L. Bai, X.D. He, Y.B. Li, C.C. Zhu, S. Zhang, J. Mater. Res. 24 (2009) 2528–2535.
[14] Y.C. Zhou, J.X. Chen, J.Y. Wang, Acta Mater. 54 (2006) 1317–1322.
[15] M. Radovic, M.W. Barsoum, A. Ganguly, T. Zhen, P. Finkel, S.R. Kalidindi, E. Lara-Curzio, Acta Mater. 54 (2006) 2757–2767.
[16] H.B. Zhang, Y.C. Zhou, Y.W. Bao, M.S. Li, Acta Mater. 52 (2004) 3631–3637.
[17] T. Scabarozi, A. Ganguly, J.D. Hettinger, S.E. Lofland, S. Amini, P. Finkel, T. El-Raghy, M.W. Barsoum, J. Appl. Phys. 104 (073713) (2008) 1–6.
[18] Y.C. Zhou, F.L. Meng, J. Zhang, J. Am. Ceram. Soc. 91 (2008) 1357–1360.
[19] W.B. Tian, Z.M. Sun, H. Hashimoto, Y.L. Du, J. Alloy Compd. 484 (2009) 130–133.
[20] Z.M. Sun, R. Ahuja, J.M. Schneider, Phys. Rev. B 68 (22412) (2003) 1–4.
[21] Z.J. Lin, M.S. Li, J.Y. Wang, Y.C. Zhou, J. Am. Ceram. Soc. 90 (2007) 3930–3937.
[22] F. Chung, J. Appl. Crystallogr. 7 (1974) 519–525.
[23] B. Hallstedt, D. Music, Z. Sun, Int. J. Mater. Res. 97 (2006) 539–542.
[24] N.V. Tzenov, M.W. Barsoum, J. Am. Ceram. Soc. 83 (2000) 825–832.
[25] Z.J. Lin, M.S. Li, J.Y. Wang, Y.C. Zhou, Acta Mater. 55 (2007) 6182–6191.
[26] R. Fourmentin, M.N. Avettand-Fenoel, G. Reumont, P. Perrot, J. Mater. Sci. 42 (2007) 7934–7938.
[27] X.H. Wang, Y.C. Zhou, Acta Mater. 50 (2002) 3141–3149.
[28] W.B. Tian, P.L. Wang, G.J. Zhang, Y.M. Kan, Y.X. Li, D.S. Yan, Scripta Mater. 54 (2006) 841–846.
[29] P.T.B. Shaffer (Ed.), Plenum Press Hand Book of High Temperature Materials, Materials Index, vol. 1, Plenum, New York, 1964.
[30] J.X. Chen, J.L. Li, Y.C. Zhou, J. Mater. Sci. Technol. 22 (2006) 455–458.